Inorganic Chemistry

Article

pubs.acs.org/IC

Proton-Assisted Mechanism of NO Reduction on a Dinuclear Ruthenium Complex

Tatsuya Suzuki,[†] Hiromasa Tanaka,[‡] Yoshihito Shiota,[†] P. K. Sajith,[†] Yasuhiro Arikawa,*[,§] and Kazunari Yoshizawa*[,†,‡]

[†]Institute for Materials Chemistry and Engineering and International Research Center for Molecular System, Kyushu University, Nishi-ku, Fukuoka 819-0395, Japan

[‡]Elements Strategy Initiative for Catalysts and Batteries, Kyoto University, Nishikyo-ku, Kyoto 615-8245, Japan

[§]Division of Chemistry and Materials Science, Graduate School of Engineering, Nagasaki University, Bunkyo-machi 1-14, Nagasaki 852-8521, Japan

Supporting Information

ABSTRACT: Density-functional-theory (DFT) calculations are performed for the proposal of a plausible mechanism on the reduction of NO to N_2O by a dinuclear ruthenium complex, reported by Arikawa and co-workers [*J. Am. Chem. Soc.* **2007**, *129*, 14160]. On the basis of the experimental fact that the reduction proceeds under strongly acidic conditions, the role of protons in the mechanistic pathways is investigated with model complexes, where one or two NO ligands are protonated. The reaction mechanism of the NO reduction is partitioned into three steps: reorientation of N_2O_2 (*cis*-NO dimer), O—N bond cleavage, and N_2O elimination. A key finding is that the protonation of the NO ligand(s) significantly reduces the activation barrier in the rate-determining reorientation step. The activation energy of 43.1 kcal/mol calculated for the proton-free model is reduced to 30.2 and 17.6 kcal/mol for the mono- and diprotonated models, respectively. The protonation induces the electron transfer from the Ru(II)Ru(II) core to the O═N—N═O moiety to give a Ru(III)Ru(III) core and a hyponitrite $(O—N═N—O)^{2-}$ species. The formation of the hyponitrite species provides an alternative pathway for the N_2O_2 reorientation, resulting in the lower activation energies in the presence of proton(s). The protonation also has a marginal effect on the O—N bond cleavage and the N_2O elimination steps. Our calculations reveal a remarkable role of protons in the NO reduction via N_2O formation and provide new insights into the mechanism of NO reduction catalyzed by metalloenzymes such as nitric oxide reductase (NOR) that contains a diiron active site.

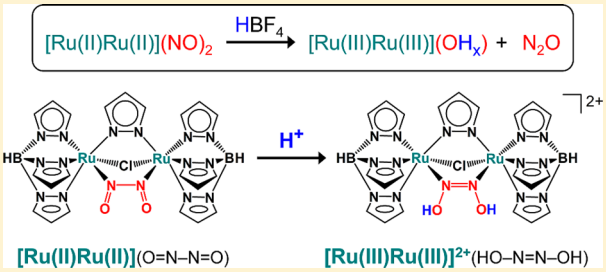

INTRODUCTION

During the last two decades, the transition metal complexes containing NO ligand have received great attention, due to the recognition that the reactions and electronic structures of such complexes can provide useful insights into the fundamental physiological roles of NO associated with neurotransmission, blood pressure, and immune systems.[1−3] The intricate chemistry of metal nitrosyl complexes is often related with the noninnocent behavior of NO. In metal nitrosyl complexes, NO usually displays three different oxidation states, which can be viewed as NO^+ (linear form), NO (half-bent form), and NO^- (bent form).[4−10] A recent discovery showed that NO can also exist in the dianionic form, NO^{2-}, when it is bridged between two yttrium metal centers.[11] Understanding the reactions of NO is of great interest from both biological and environmental viewpoints. NO has been identified as an intermediate in the biological denitrification process, which involves the reduction of nitrate into dinitrogen. During that process, the metalloenzyme nitric oxide reductase (NOR) catalyzes the two-electron reduction of NO to N_2O, as shown in eq 1.

$$2NO + 2H^+ + 2e^- \rightarrow N_2O + H_2O \quad (1)$$

It is clear that the formation of an N−N bond and the cleavage of an N−O bond are involved in the NO reduction reaction. The active center of NOR contains two Fe atoms, where one is a heme and the other is a nonheme group.[12−14] The same reaction can also be mediated by the enzyme cytochrome *c* oxidase (CcO) with a bimetallic active site of Cu and Fe (heme) atoms.[14−18] Great efforts have been devoted to unraveling the mechanism of NO reduction by NORs with both experimental and theoretical approaches.[19−31]

A scavenging nitric oxide reductase (s-NOR), which is an A-type flavoprotein (FprA) in *Moorella thermoacetica*, works as a NO radical scavenger under anaerobic conditions.[32,33] Figure 1a shows the active site of s-NOR containing a nonheme diiron

Received: February 18, 2015
Published: July 17, 2015

DOI: 10.1021/acs.inorgchem.5b00394
Inorg. Chem. 2015, 54, 7181−7191

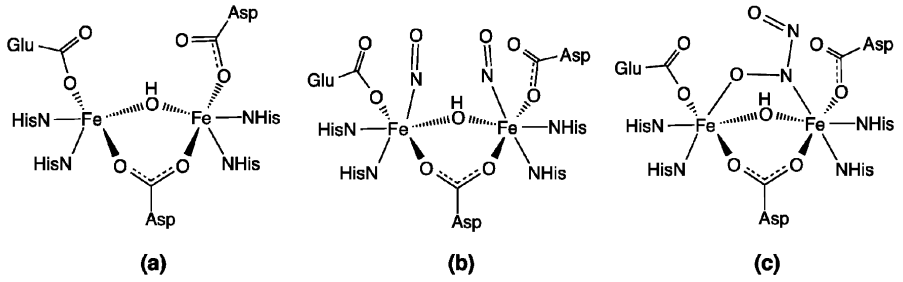

Figure 1. Schematic representation of the active site (a) and the proposed intermediates (b, c) in s-NOR.

complex, in which the two iron atoms are connected with a carboxylate ligand and a hydroxido ligand. Silaghi-Dumitrescu et al. reported that their X-ray crystal structure of the diiron site of s-NOR has a vacant coordination site for two incoming NO molecules and expected the formation of a dinitrosyl diiron structure (Figure 1b), although NO adducts of s-NOR have not been observed.[32] They also commented that the size of the substrate binding pocket is large enough to consider a mononitrosyl diiron structure, where one NO is coordinated to the diiron site and a second noncoordinating NO sits above the site. On the basis of theoretical calculations using a cluster model, Blomberg et al. suggested that an ON-bridged NO dimer coordination (Figure 1c) is energetically more favorable than the dinitrosyl coordination.[34] They also proposed that the NO reduction at the active site of s-NOR starts with the coordination of a single NO molecule to the diiron core in a μ-κ^1(O):κ^1(N) fashion, and then another molecule of NO attacks the bridging NO ligand to form the ON-bridged *cis*-NO dimer. However, very recently, Caranto et al. reported the detection of a new transient intermediate, a structurally and electronically symmetrical antiferromagnetically coupled $[\{FeNO\}^7]_2$.[35] On the basis of their multispectroscopic pre-steady-state investigation, they proposed that the N—N bond formation and N—O bond cleavage originate from this dinitorsyl diiron structure. Zheng et al. recently prepared a dinitrosyl diiron complex $[Fe_2(BPMP)(OPr)(NO)_2](BPh_4)_2$ involving weakly electronically coupled $\{FeNO\}^7$ units.[36] This complex can be considered as a functional model of NORs since nearly quantitative evolution of N_2O was observed by two-electron reduction.

A relevant question about the role of protons in the NO reduction process still remains unanswered. Since the NO reduction mediated by NORs consumes two protons to yield N_2O ($2NO + 2H^+ + 2e^- \rightarrow N_2O + H_2O$), the involvement of protons in the N_2O formation step in the NO reduction is a matter of debate.[16,17,25,37−42] A family of NOR, ba_3-oxidoreductase from *Thermus thermophilus*, is also known as an enzyme that catalyzes the transformation of NO to N_2O under anaerobic conditions. This enzyme has a heme iron−copper bimetallic structure at the activation site. On the basis of resonance Raman spectroscopy measurements and theoretical calculations, Varotsis and co-workers proposed a reaction pathway for the NO reduction that a protonated hyponitrite species ($HONNO^-$) is transiently formed under reducing conditions.[16,17,41,42] In their proposal, the initial binding of two NO molecules to the bimetallic active site is followed by protonation of the coordinated NO species and concomitant formation of the N—N bond. Very recently, we have shown that protons can play a significant role in the decomposition of NO ($2NO \rightarrow N_2 + O_2$) catalyzed by a copper ion-exchanged zeolite Cu-ZSM-5, where N_2O is one of the important intermediates in the catalytic cycle.[43]

Arikawa and co-workers[44,45] recently synthesized a dinuclear ruthenium complex $[(TpRu)_2(\mu\text{-Cl})(\mu\text{-pz})\{\mu\text{-N}(=O)—N(=O)\text{-}\kappa^2\}]$ (**A**), where Tp is hydridotris(pyrazolyl)borate ligand, as shown in Figure 2. They observed an N—N coupling of the

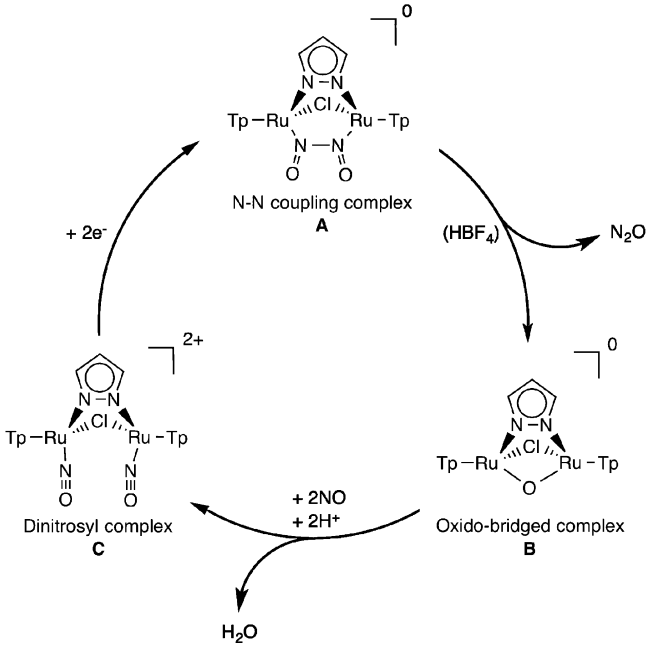

Figure 2. NO reduction cycle formally achieved by dinuclear ruthenium complexes.

two neighboring NO ligands in **A** by two-electron reduction of a dinitrosyl complex $[\{TpRu(NO)\}_2(\mu\text{-Cl})(\mu\text{-pz})]^{2+}$ (**C**) at room temperature. Treatment of **A** with 1.1 equiv of $HBF_4\cdot OEt_2$ afforded an oxido-bridged complex $[(TpRu)_2(\mu\text{-Cl})(\mu\text{-O})(\mu\text{-pz})]$ (**B**) in 21% yield with evolution of N_2O. They also confirmed mono- and diprotonation of the oxido bridge in **B** by HBF_4, leading to replacement of the oxido bridge by two molecules of NO to yield **C**. Hence, the NO reduction cycle can be achieved in this diruthenium system. Experimental observations suggest that the protonation of the NO ligand(s) by a strong acid such as HBF_4 should be essential for the NO reduction on the diruthenium complex. This NOR-type reaction can open a way to gain better insights into the NO reduction reactions mediated by a bimetallic active center. Here we consider mechanistic details of the NOR-type reaction by a dinuclear ruthenium complex. To elucidate the role of proton in the NO reduction process, the mechanism of the transformation of NO into N_2O on the diruthenium complex has been theoretically investigated by using proton-free and protonated models, the latter of which involves protonated NO

DOI: 10.1021/acs.inorgchem.5b00394
Inorg. Chem. 2015, 54, 7181−7191

Scheme 1. Proton-Free, Monoprotonated, and Diprotonated Models of Complex A

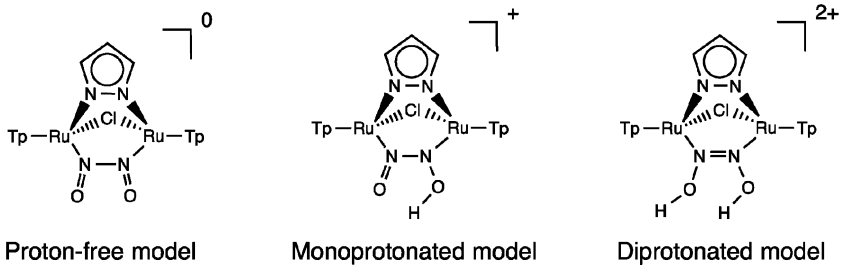

Table 1. Selected Geometrical Parameters of A–C in the Singlet State Optimized at the B3LYP/SDD/D95 Level of Theory[a]**

	A		B		C	
	calcd[a]	exptl[b]	calcd	exptl[b]	calcd	exptl
			Distances (Å)			
Ru–Ru	3.607 (3.520)	3.5455(2)	3.087[d]	3.0491(6)	3.829	3.6935(9)
Ru–N[c]	1.891 (2.035)	1.866(2)			1.760	1.713(7)
						1.766(7)
N–N	1.849 (1.443)	1.856(3)			3.146	3.006(9)
N–O[c]	1.197 (1.242)	1.190(2)			1.156	1.169(10)
						1.131(9)
Ru–O[c]			1.915[d]	1.898(4)		
				1.904(3)		
			Bond Angles (deg)			
Ru–N–O[c]	135.9 (124.3)	136.9(2)			170.0	169.7(7)
						165.4(6)
ν(NO) (cm^{-1})	1715 (1477)	1608			1988	1928

[a]Parameters in the low-lying triplet state are given in parentheses. Corresponding experimental values are taken from their X-ray crystal structures.[44] [b]Two ruthenium atoms are connected with 4-bromopyrazole, instead of pyrazole. [c]Averaged values in the optimized structures. [d]Open-shell singlet state.

ligand(s). We compare reaction pathways calculated with these models and demonstrate that the involvement of protons effectively accelerates key reaction steps toward the formation of N_2O.

2. METHOD OF CALCULATION

In the present study, the N–N coupling complex in Figure 2 was chosen as the initial complex for exploring reaction pathways for the transformation of two molecules of NO into N_2O. To take account of the strongly acidic conditions during the reaction, the mechanism has been investigated for three forms of the N–N coupling complex, *viz.*, proton-free, monoprotonated, and diprotonated models, as shown in Scheme 1. In the first model, no proton is incorporated to the two NO ligands on the diruthenium core, while in their monoprotonated and diprotonated models, one and two protons bound to the NO dimer, respectively.

Density-functional-theory (DFT) calculations were performed with the Gaussian 09 program package.[46] Geometry optimization and transition-state search were carried out with the B3LYP method[47−49] combined with the SDD basis set[50] for Ru atoms and D95** basis sets[51] for the other atoms. Vibrational analyses were carried out for all reaction species to characterize stationary-point structures. An appropriate connection between a reactant and a product was confirmed by intrinsic reaction coordinate (IRC) calculations.[52−54] Three possible spin states, the closed-shell singlet, open-shell singlet, and triplet states, were examined in searching for the reaction pathways. The open-shell singlet state was calculated by using the broken-symmetry approach. Solvent effects of dichloromethane (ε = 8.93) were evaluated with single-point energy calculations at the gas-phase-optimized geometries using the polarizable continuum model (PCM).[55] Energy profiles of the calculated reaction pathways are presented as Gibbs free energy changes (ΔG's) involving thermal corrections at 298.15 K.

3. RESULTS AND DISCUSSION

3.1. Geometric and Electronic Structures of Dinitrosyl Complexes. Table 1 summarizes geometric parameters of complexes **A**–**C** optimized at the B3LYP level of theory. The electronic ground state is singlet for **A**–**C**, which is consistent with the experimental observation that they all showed diamagnetism.[44,45] The geometric parameters of **A**–**C** in the singlet state reasonably reproduce the corresponding experimental values.

Prior to the discussion on the calculated reaction pathway starting from **A**, we would like to compare geometric and electronic structures of **A** with **C**. For both the complexes the electronic ground state is the closed-shell singlet. The triplet and quintet states of **A** lie 17.6 and 45.2 kcal/mol above the closed-shell singlet state, while the open-shell singlet, triplet, and quintet states of **C** are higher in energy by 25.9, 26.4, and 41.7 kcal/mol, respectively. The open-shell singlet state of **A** was relaxed to the closed-shell one after optimization. The two-electron reduction of **C** yielding **A** significantly decreases the N–N distance from 3.146 to1.849 Å in the closed-shell singlet state, the latter of which is much longer than a typical single N–N bond distance of 1.42 Å[56] to be rather close to that of a free NO dimer in the gas phase (1.951 Å at the B3LYP/D95* level of theory). The Mayer bond orders[57,58] of the N–N bond in **C** and **A** are calculated to be 0.00 and 0.47, respectively. The calculated N–N bond distances and bond orders indicate that the reduction of **C** provides a weak bonding interaction between the nitrogen atoms of the NO ligands. The geometric change during the two-electron reduction can be understood by looking at the frontier orbitals of **A** and **C** (Figure 3a). The

DOI: 10.1021/acs.inorgchem.5b00394
Inorg. Chem. 2015, 54, 7181−7191

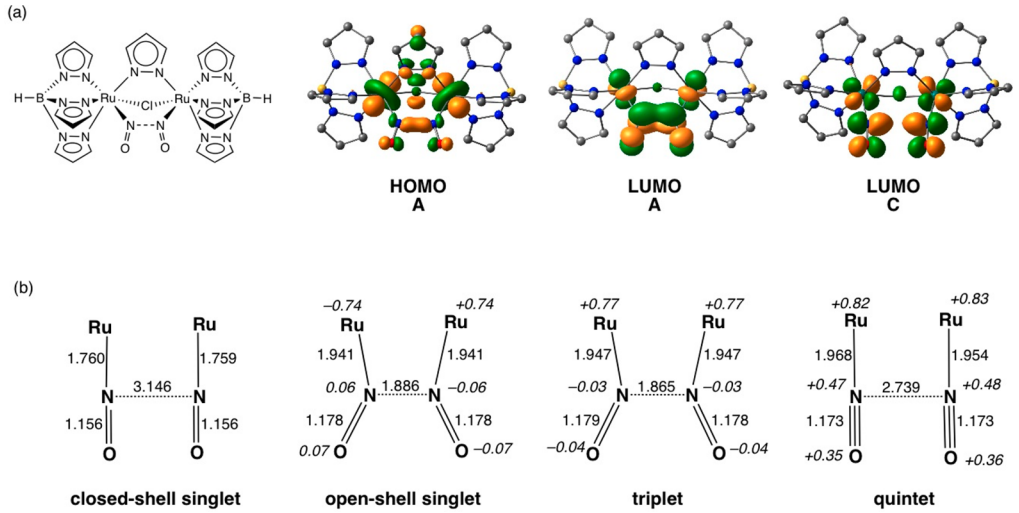

Figure 3. (a) Frontier orbitals of the closed-shell singlet state of **A** and **C**. (b) Interatomic distances in Å and Mulliken spin densities (in italics) assigned to the $Ru_2(NO)_2$ moiety in the closed-shell singlet, open-shell singlet, triplet, and quintet states of **C**.

HOMO of **A** shows an in-plane overlap of the π^* orbitals of the NO ligands. The spatial distribution of the HOMO in the vicinity of the NO ligands is very similar to that of a *cis*-NO dimer. On the other hand, the HOMO of **A** corresponds to the LUMO of the dicationic complex **C**, and hence the two NO ligands in **C** have no bonding interaction between them.

As shown in Chart 1, each Ru−NO moiety in **C** can have various electronic structures, such as Ru(II)—(N≡O)$^+$,

Chart 1. Possible Electronic Structures of a Pair of Nitrosyl Ligands Coordinated to the Diruthenium Core of (a) A and (b) C

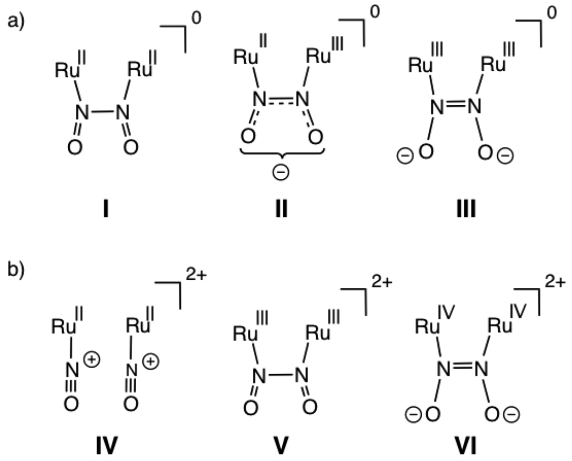

Ru(III)—(N═O)$^\bullet$, and Ru(IV)—(N═O)$^-$. Figure 3b presents the Mulliken spin densities assigned to the Ru atoms and NO ligands in the open-shell singlet, triplet, and quintet states of **C**. For all the spin states, each Ru atom possesses a spin density of about 0.7, and thus the formal charge of Ru should be regarded as +3. It is notable that the NO ligands in the open-shell singlet and triplet states have negligibly small spin densities due to the formation of a *cis*-NO dimer, while a spin density of about 0.6 (triplet) is assigned to the remaining ligands. Thus, two Ru(III) atoms in the open-shell singlet and triplet states are coupled antiferromagnetically and ferromagnetically, respectively. The formation of *cis*-NO dimer in the open-shell singlet allows us to exclude an electronic structure of the singlet state with an antiferromagnetic coupling between a low-spin Ru(III) and (NO)$^\bullet$. In addition, a possibility of the combination of a low-spin Ru(IV) and NO$^-$ can be ruled out by the long N—N distance in **C** (3.146 Å) because a pair of NO$^-$ can form a hyponitrite structure ($^-$O—N═N—O$^-$) with a strong N═N bond, such as structure **VI** in Chart 1. From these results, the electronic structure of the $Ru_2(NO)_2$ moiety in the open-shell singlet and triplet states of **C** should be described as structure **V**, $[Ru(III)]_2(N_2O_2)$, in Chart 1. Concerning the ground state (the closed-shell singlet state) of **C**, on the other hand, the linear Ru−NO moiety (ca. 170°) as well as the very long N—N distance (>3 Å) in the crystal and optimized structures suggest that the electronic structure of NO should be described as NO$^+$ because a couple of neutral NO$^\bullet$ species should form a *cis*-NO dimer, where the N—N distance is about 1.8 Å. This means that each ruthenium atom receives an electron from the NO ligand to form the Ru(II)—NO$^+$ moiety. However, the distance and vibrational frequency of the N—O bond in the optimized **C** are 1.156 Å and 1988 cm^{-1}, which are close to those of NO$^\bullet$ (1.167 Å and 1959 cm^{-1} at the B3LYP/D95* level) rather than NO$^+$ (1.081 Å and 2432 cm^{-1}). Merkle et al. recently reported that strong π-back bonding causes a distinct lowering of the N—O stretching frequency in Ru(II)—NO$^+$ complexes bearing tris(2-pyridylmethyl)amine as an ancillary ligand.[59] On the basis of all the calculated results, the electronic structure of the $Ru_2(NO)_2$ moiety in the closed-shell singlet state of **C** can be described as structure **IV**, $[Ru(II)(NO^+)]_2$, in Chart 1.

The electronic structure of the Ru−NO moiety in **A** also depends on its spin state. As described above, two-electron reduction of **C** results in the significant shortening of the N−N distance between the two NO ligands in the ground spin state (the closed-shell singlet) of **A**. The in-plane overlap between the π^* orbitals of the NO ligands in the HOMO provides a weak bond interaction between the two nitrogen atoms. The N−N distance (Mayer bond order) between the NO ligands of 1.849 Å (0.58) in the closed-shell singlet state of **A** is close to that of a free *cis*-NO dimer (1.951 Å (0.47)), implying that the two NO ligands are coordinated to the diruthenium core as a neutral *cis*-NO dimer. In addition, the Ru−N and N−O distances in the closed-shell singlet state of **A** are calculated to

DOI: 10.1021/acs.inorgchem.5b00394
Inorg. Chem. 2015, 54, 7181−7191

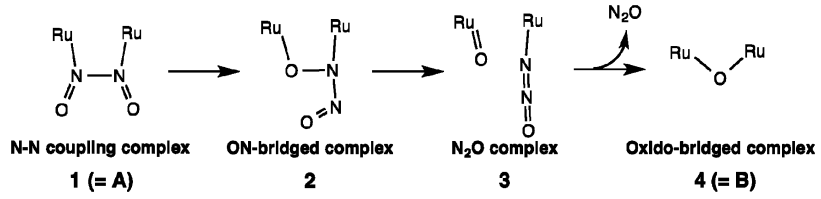

Figure 4. Reaction mechanism of NO reduction on the diruthenium complex.

	1	$TS_{1/1a}$	1a	$TS_{1a/1b}$	1b	$TS_{1b/2}$	2	$TS_{2/3}$	3	$TS_{3/4}$	4
Ru^a	0.80	0.30	0.29	0.19	0.80	0.79	0.72	1.03	1.07	1.08	0.72
Ru^b	0.23	0.83	0.84	0.76	0.31	0.35	0.65	0.13	0.00	0.01	0.70
N^a	0.20	0.00	0.00	0.18	0.56	0.45	0.06	−0.12	0.00	0.00	
N^b	0.05	0.20	0.21	0.12	−0.07	0.00	0.05	0.18	0.00	0.00	
O^a	0.36	0.18	0.16	0.24	0.31	0.24	0.18	0.48	0.91	0.89	0.53
O^b	0.19	0.31	0.32	0.32	0.01	0.08	0.24	0.22	0.00	0.00	

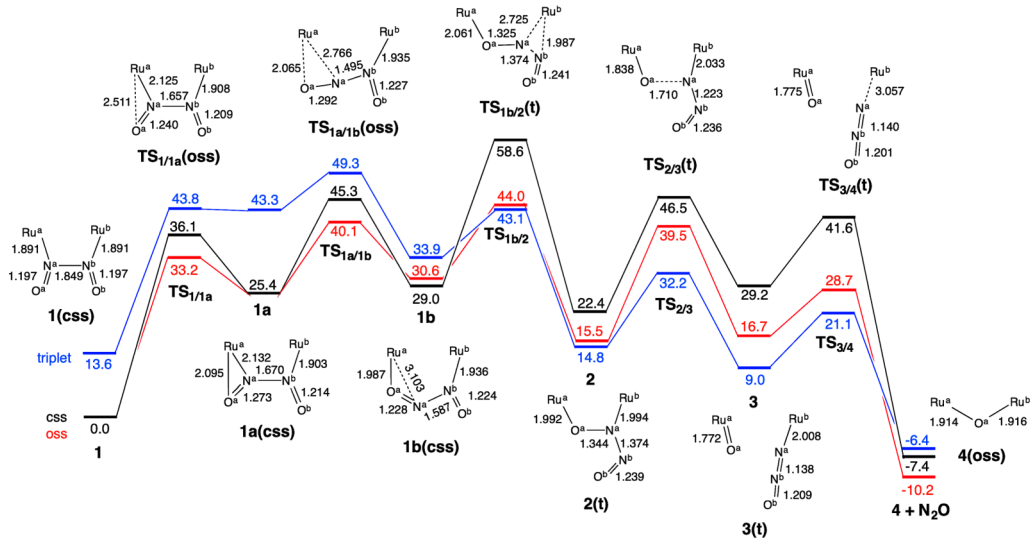

Figure 5. Energy diagrams and optimized structures along the proton-free path. Distances and the Gibbs free energy changes (ΔG's) at room temperature are presented in Å and kcal/mol, respectively. Mulliken spin densities in the triplet state are shown in the table.

be 1.891 and 1.197 Å (Table 1), which are close to those of the open-shell singlet state of **C** (1.941 and 1.178 Å) rather than the closed-shell singlet state (1.760 and 1.156 Å) (Figure 3b). As described above, the electronic structure of each Ru−NO moiety in **C** can be described as Ru(III)−$NO^{\bullet}$ in the open-shell singlet state and Ru(II)−NO^+ in the closed-shell singlet state. These geometric parameters indicate that two electrons added to the closed-shell singlet state of **C** are utilized for reducing a couple of the NO^+ ligands to afford a neutral NO dimer in the closed-shell singlet state of **A**. The instability of the open-shell singlet state denies the antiferromagnetic coupling between the diruthenium core and the NO dimer or between the Ru−NO moieties, and thus the Ru_2−N_2O_2 moiety in the closed-shell singlet state of **A** can be described as $[Ru(II)]_2(N_2O_2)$ (structure **I** in Chart 1). This electronic structure apparently differs from that of a dinitrosyl diiron intermediate $[\{FeNO\}^7]_2$ observed in NO reduction catalyzed by a flavo-diiron protein, in which two $\{FeNO\}^7$ units are antiferromagnetically coupled.[35] In the triplet state of **A**, on the other hand, the N−N bond distance is significantly shortened (1.443 Å), and the N−O vibrational frequency is red-shifted from 1715 to 1477 cm^{-1}. The N−N bond distance in the triplet state is close to that of an anionic *cis*-$N_2O_2^-$ (1.403 Å at the B3LYP/D95* level), and the Mulliken spin density of 0.80 is assigned to the N_2O_2 moiety. The unpaired electron in the N_2O_2 moiety accommodates a molecular orbital corresponding to the LUMO of the singlet state (Figure 3a), and thereby the N−N bond of the N_2O_2 moiety is strengthened through the out-of-plane overlap of π^* orbitals of the NO ligands. On the other hand, the sum of the spin densities assigned to the diruthenium core (0.96) indicates that the diruthenium core possesses one unpaired electron, but the spin densities are unequally distributed on each Ru atom (0.23 and 0.73) in spite of the highly symmetrical geometry. The distribution of the spin densities in the triplet state of **A** shows that the diruthenium core has a mixed-valent Ru(II)Ru(III) character (structure **II**, $[Ru(II)Ru(III)]^+(N_2O_2)^-$, in Chart 1). In the triplet state, two electrons added to **C** are separately located at the diruthenium core and the N_2O_2 moiety.

3.2. Proton-Free Mechanism of NO Reduction. Figure 4 presents a plausible reaction pathway for the NO reduction starting from **1**. In the following discussion, complexes **A** and **B** are denoted as complexes **1** and **4**, respectively. Reorientation of the O—N—N—O moiety in **1** results in an O—N-bridged complex **2**, which is ready for the cleavage of the bridging O—N bond. The O—N bond cleavage of **2** leads to the formation of N_2O and a ruthenium-oxido (Ru═O) complex **3**. Finally,

DOI: 10.1021/acs.inorgchem.5b00394
Inorg. Chem. 2015, 54, 7181−7191

the N_2O molecule is released from the diruthenium core to afford the oxido-bridged complex **4**.

Figure 5 shows energy diagrams of the reaction pathway of different spin states for the NO reduction starting from **1** without proton on the NO ligands, together with optimized structures of the Ru_2—(N_2O_2) moiety of the intermediates and transition states. Reorientation of the NO dimer in **1** involves three elementary steps: (i) One of the end-on coordinated NO ligands changes its coordination to a side-on manner to form intermediate **1a**. (ii) A *cis*-to-*trans* isomerization of the NO dimer affords an N—N—O-bridged intermediate **1b**. (iii) Recombination of the Ru—N bonds yields the O−N-bridged intermediate **2**. The change of coordination manner in step i via $\mathbf{TS_{1/1a}}$ proceeds in an endergonic way by 25.4 kcal/mol with a high activation energy of 33.2 kcal/mol. Interestingly, the ground spin state of $\mathbf{TS_{1/1a}}$ is an open-shell singlet state, whereas those of **1** and **1a** are found to be closed-shell singlet states. The triplet state of **1a** is 17.9 kcal/mol above the singlet state, and the open-shell singlet state was not obtained due to high stability of the closed-shell singlet state. In step ii, the coordinated N_2O_2 dimer undergoes a *cis*-to-*trans* isomerization to give **1b** via $\mathbf{TS_{1a/1b}}$. As a result, the Ru^a—N^a bond is completely cleaved to form a *trans*-NO dimer. This step is slightly endergonic by 3.6 kcal/mol with an activation energy of 14.7 kcal/mol. The approach of O^a to Ru^a during the isomerization temporally forces the shortening of the N—N bond (1.849 Å (**1**) → 1.670 Å (**1a**) → 1.587 Å (**1b**)), enhancing the $Ru(III)_2$—$(O—N{=}N—O)^{2-}$ character of the Ru_2−(N_2O_2) moiety. In step iii, the formation of the Ru^b—N^a bond synchronizes with the cleavage of Ru^b—N^b bond to give the O—N-bridged intermediate **2** via $\mathbf{TS_{1b/2}}$. In this reaction step, $\mathbf{TS_{1b/2}}$ and the resultant **2** adopt a triplet state as the ground spin state, and the barrier height in the closed-shell singlet state (29.6 kcal/mol) is too high to overcome at room temperature. The low-lying triplet state of $\mathbf{TS_{1b/2}}$ (43.1 kcal/mol) compared to the closed-shell singlet state (58.6 kcal/mol) indicates that these potential energy surfaces are crossed in the vicinity of $\mathbf{TS_{1b/2}}$. Such a spin inversion between the singlet and triplet states can reduce the activation energy from 29.6 to 14.1 kcal/mol. The dihedral angle of O^a—N^a—N^b—O^b is decreased from 165.5° in the closed-shell singlet state of **1b** to 43.6° in the triplet state of $\mathbf{TS_{1b/2}}$. This geometrical change reflects the *trans*-to-*cis* isomerization of NO dimer, leading to the O—N-bridged intermediate **2** bearing the *cis*-NO dimer. The N—N bond distance of **2** in the triplet state (1.374 Å) is significantly shorter than that of **1** in the singlet state (1.849 Å), while the O^a—N^a bond distance is elongated by 0.147 Å (1.197 Å → 1.344 Å). These geometric changes as well as the Mulliken spin densities assigned to Ru^a (0.72) and Ru^b (0.65) in **2** can be associated with the reduction of the N_2O_2 moiety by the Ru(II)−Ru(II) core.

After the reorientation, the activated O^a—N^a bond in **2** is split to yield intermediate **3** containing the Ru—NNO and Ru═O moieties via $\mathbf{TS_{2/3}}$. The O—N bond cleavage in the triplet state is an exergonic reaction (ΔG = −5.8 kcal/mol) with an activation energy of 17.4 kcal/mol. Spin densities of 0.48 and 0.28 are assigned to O^a and $N^aN^bO^b$ in the triplet state of $\mathbf{TS_{2/3}}$, respectively, indicating homolysis of the O—N bond cleavage. After the O—N bond cleavage, spin densities are localized at Ru^a (1.07) and O^a (0.91), and hence the Ru^b—$N^aN^bO^b$ moiety in **3** has a closed-shell singlet character. Once the N_2O ligand in **3** is released from Ru^b, the oxido ligand on Ru^a is spontaneously shared by the two ruthenium atoms to give the oxido-bridged complex **4**. The activation energies calculated for the three spin states are almost identical (12.0−12.4 kcal/mol). The barrier in this reaction step would be responsible for the Ru—NNO bond cleavage because the Ru—NNO moiety has a common geometric and electronic structure in all spin states; see Supporting Information Figure S1 for the singlet state structures. We confirmed that the structure of **3** in the absence of N_2O was relaxed to **4** with no activation barrier. The final step toward the NO reduction (**3** → **4** + N_2O) proceeds in an exergonic way by 15.4 kcal/mol in the triplet state, while the triplet state of **4** lies 3.8 kcal/mol above the open-shell singlet state that is experimentally proposed. Therefore, the potential energy surfaces of the singlet and triplet states should cross again in the vicinity of $\mathbf{TS_{3/4}}$.

In summary, the energy profile of the NO reduction along with the proton-free path demonstrates that the total reaction **1** → **4** + N_2O is exergonic by 10.2 kcal/mol in the singlet state. However, the reorientation of the N_2O_2 ligand is a highly energy-demanding process that requires at least 43.1 kcal/mol to obtain the O−N-bridged intermediate **2**. We can thus conclude that the NO reduction at the diruthenium core does not occur under mild conditions in the absence of proton. These results are fully consistent with experimental observations.[44,45]

3.3. Proton-Assisted Mechanisms. The energy profile calculated for the proton-free model clearly shows that the reorientation of the NO dimer at the diruthenium core would not proceed at room temperature. From the experimental fact that a strong acid (HBF_4) was required for the NO reduction,[44,45] we examine two possible reaction pathways starting from the mono- and diprotonated N−N coupling complexes **1**[H] and **1**[2H], in which one and two NO ligands in **1** are protonated, respectively. First, we would like to validate the protonated models adopted here. As seen in the HOMO of **A** (**1**) in Figure 3a, the nitrogen atoms of the bridging pyrazole and chlorine ligands are also likely to accept a proton. As summarized in Supporting Information Table S1, the oxygen atoms of the NO ligands are energetically the most favorable basic site for both the first and second protonations. The second point to be assessed is the heat balance of the first and second protonation reactions in the presence of HBF_4 as an acid. We first calculated the proton transfer from HBF_4 to an NO ligand in **1**, but failed due to difficulty in optimizing a neutral $HF{\cdots}BF_3$ species involved in the complex of **1** and HBF_4. In the present study we have evaluated the heat balance for the protonation reactions using CF_3SO_2OH (pK_a = −11.5 in 1,2-dichloroethane) instead of HBF_4 (pK_a = −10.3).[60,61] The protonation of **1** (**1** + CF_3SO_2OH → **1**[H] + $CF_3SO_3^-$) is calculated to be exergonic by 4.1 kcal/mol, while the protonation of **1**[H] (**1**[H] + CF_3SO_2OH → **1**[2H] + $CF_3SO_3^-$) is endergonic by 4.3 kcal/mol. Optimized structures for the protonation by CF_3SO_2OH are presented in Supporting Information Figure S2. These calculational results suggest that one of the NO ligands in **1** should be protonated in the presence of a strong acid, and the protonation of the remaining NO ligand is also possible. The experimental fact[44] that the evolution of N_2O was achieved by the use of 1.1 equiv of HBF_4 supports that the second protonation can occur at least temporarily. As described later, the calculated energy profiles indicate that the protonation of both NO ligands in **1** should be essential only at the first step of the NO reduction (reorientation step).

DOI: 10.1021/acs.inorgchem.5b00394
Inorg. Chem. 2015, 54, 7181−7191

	1[H]	$TS_{1/1c}$[H]	1c[H]	$TS_{1c/2}$[H]	2[H]	$TS_{2/3}$[H]	3[H]	$TS_{3/4}$[H]	4[H]
Ru^a	0.84	0.82	0.84	0.80	0.84	0.85	0.81	0.81	0.85
Ru^b	0.77	0.82	0.84	0.82	0.81	0.80	0.75	0.78	0.85
N^a	0.04	0.01	0.00	0.01	0.05	0.01	0.00	0.00	
N^b	−0.06	−0.03	−0.01	−0.01	−0.04	−0.03	−0.01	0.00	
O^a	0.11	0.03	−0.01	0.03	0.02	0.05	0.01	0.00	0.07
O^b	−0.01	-0.01	0.00	0.00	0.04	0.04	0.19	0.18	

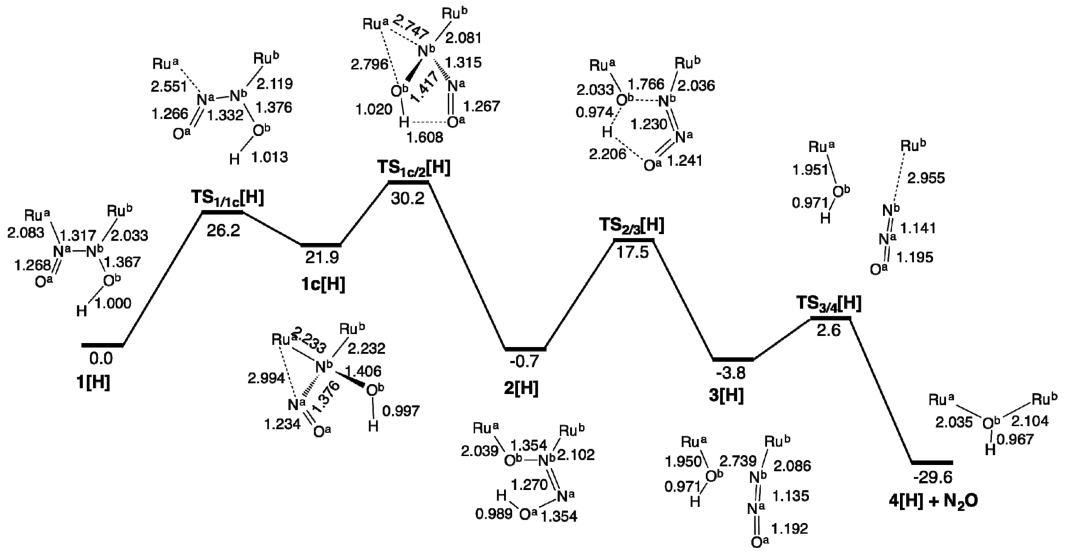

Figure 6. Energy diagrams and optimized structures for the NO reduction by monoprotonated complex **1**[**H**] in the triplet state. Distances and Gibbs free energy changes (ΔG's) at room temperature are presented in Å and kcal/mol, respectively. Mulliken spin densities are presented in the table.

	1[2H]	$TS_{1/2}$[2H]	2[2H]	$TS_{2/5}$[2H]	5[2H]	$TS_{5/3}$[2H]	3[2H]	$TS_{3/4}$[2H]	4[2H]
Ru^a	0.76	0.79	0.80	1.04	1.40	1.33	0.83	0.83	0.80
Ru^b	0.79	0.79	0.78	0.64	0.04	0.14	0.77	0.79	0.80
N^a	−0.02	0.01	0.00	−0.03	−0.01	−0.04	0.00	0.00	
N^b	0.00	−0.01	−0.01	−0.18	−0.03	−0.06	−0.01	0.00	
O^a	0.00	0.00	0.00	−0.03	−0.01	0.00	0.01	0.00	0.00
O^b	0.00	0.00	0.00	0.09	0.27	0.07	0.00	0.01	

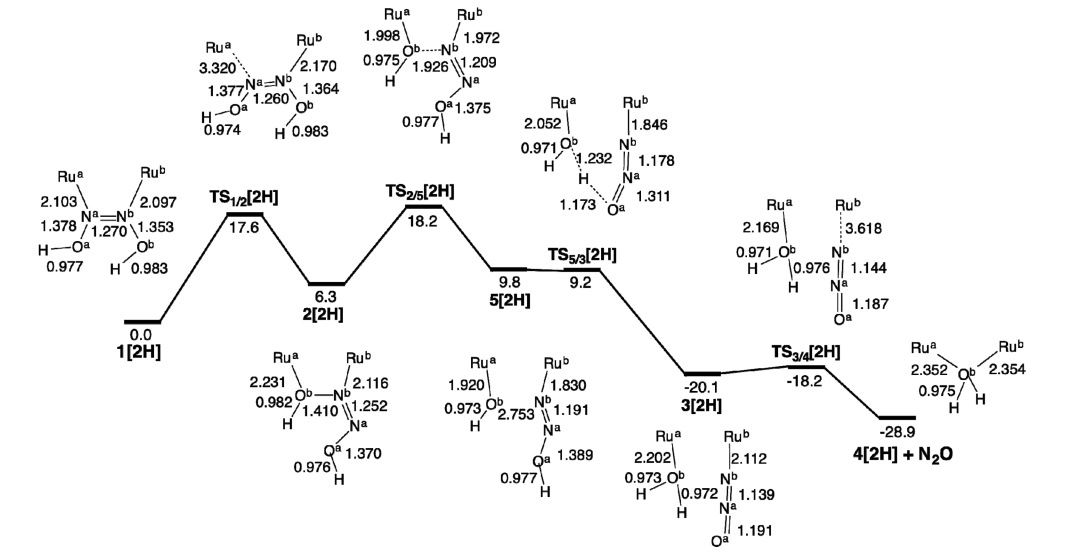

Figure 7. Energy diagrams and optimized structures for the NO reduction by diprotonated complex **1**[**2H**] in the triplet state. Distances and Gibbs free energy changes (ΔG's) at room temperature are presented in Å and kcal/mol, respectively. Mulliken spin densities are presented in the table.

It should be emphasized that the protonation of the NO ligands strongly affects both geometric and electronic structures of the Ru_2—(N_2O_2) moiety in **1**. Complexes **1**[**H**] and **1**[**2H**] in the triplet state are energetically more stable than those in

DOI: 10.1021/acs.inorgchem.5b00394
Inorg. Chem. 2015, 54, 7181−7191

the singlet state by 12.4 and 14.3 kcal/mol, respectively. The protonation significantly decreases the N—N distances from 1.849 Å (**1**) to 1.317 Å (**1**[**H**]) and 1.270 Å (**1**[**2H**]), both of which are close to the optimized N—N distance of a free *cis*-hyponitrite $(O—N{=}N—O)^{2-}$ (1.305 Å). The protonation also weakens the Ru—N bond; the average Ru−N bond distance (bond order) are varied from 1.891 Å (0.87) in **1** to 2.058 Å (0.48) in **1**[**H**] and 2.100 Å (0.37) in **1**[**2H**]. Mulliken spin densities assigned to the NO dimer are 0.08 for **1**[**H**] and −0.02 for **1**[**2H**], indicating that the N_2O_2 moiety can be regarded as $(HO—N{=}N—O)^-$ in **1**[**H**] and (HO—N=N—OH) in **1**[**2H**]. The proton(s) attached to the NO ligands thus withdraw two electrons from the Ru(II)—Ru(II) core to fix the electronic structure of $Ru(III)_2—(N_2O_2)^{2-}$. As described later, the proton-induced fixation of the hyponitrite structure prior to the reorientation step provides a great advantage in the NO reduction through the enhancement of the N—N bond.

Figures 6 and 7 present energy profiles of the NO reduction calculated along two proton-assisted pathways in the triplet state, together with optimized geometries of intermediates and transition states. The calculated energy profiles in the triplet state nearly parallel those in the open-shell singlet state, and the energy gaps between them are only 0.4−3.2 kcal/mol in the monoprotonated pathway (see Supporting Information Figures S3 and S4). The highly synchronized energy profiles of the triplet and open-shell singlet states derive from similarity in their geometric and electronic structures of the intermediates and transition states, except for ferromagnetic and antiferromagnetic nature of the diruthenium core. Thus, concerning the error range of the present DFT approach, we cannot unambiguously determine the spin state that the NO reduction proceeds in the presence of protons. Actually, for hydroxido-bridged complex **4**[**H**], the B3LYP calculations evaluated that the open-shell singlet state is 0.4 kcal/mol more stable than the triplet state, while the ^{1}H NMR of **4**[**H**] indicated paramagnetism.[45,62] In this section, we discuss only the reaction pathway in the triplet state.

The reorientation of the N_2O_2 moiety in the protonated models proceeds in a different way from that in the proton-free model. In the proton-assisted pathway, the reorientation does not go through the *cis*-to-*trans* isomerization of the N_2O_2 moiety, but is achieved by the rotation of the N_2O_2 moiety along the Ru^b−N^b bond after the Ru^a−N^a bond cleavage. For the monoprotonated model, the cleavage of the Ru^a−N^a bond in **1**[**H**] via $\mathbf{TS}_{1/1c}$[**H**] requires an activation energy of 26.2 kcal/mol. This reaction is followed by the formation of the Ru^a−N^b bond to afford **1c**[**H**], in which the two ruthenium atoms are connected with N^b. The generated **1c**[**H**] with a Ru^a−Ru^b−N^b−N^a dihedral angle of 113.7° is 21.9 kcal/mol higher in energy than **1**[**H**]; it can be regarded as a metastable intermediate in the rotation of the protonated NO dimer around the Ru^b−N^b bond leading to an O−N-bridged intermediate **2**[**H**]. The second half of the reorientation step (**1c**[**H**] → **2**[**H**]) via $\mathbf{TS}_{1c/2}$[**H**] is an exergonic reaction by 22.6 kcal/mol with an activation energy of 8.3 kcal/mol. Interestingly, the proton attached to O^b in **1c**[**H**] is concertedly migrated to O^a in **2**[**H**] through a five-membered ring structure of $\mathbf{TS}_{1c/2}$[**H**]. The highest energy point in the reorientation step is located at $\mathbf{TS}_{1c/2}$[**H**] (+30.2 kcal/mol relative to **1**[**H**]), which is lower than that in the proton-free path ($\mathbf{TS}_{1b/2}$, +43.1 kcal/mol).

The reorientation of the N_2O_2 moiety in the diprotonated path proceeds in a similar manner. However, no nitrogen-bridged intermediate such as **1c**[**H**] was optimized. IRC calculations from $\mathbf{TS}_{1/2}$[**2H**] indicated a direct connection between **1**[**2H**] and an O—N-bridged intermediate **2**[**2H**] in the reaction coordinate. The activation energy for the reorientation is calculated to be 17.6 kcal/mol, which is much lower than the highest energy point in the monoprotonated path. The calculated results on the proton-assisted paths indicate that the reorientation step should be significantly accelerated by the protonation of the NO ligands. The positive effect of the attached protons can be explained by the hyponitrite structure $(O—N{=}N—O)^{2-}$ of the N_2O_2 moiety fixed in the protonated models. The ground spin state of **1**[**H**] and **2**[**H**] is triplet with the Ru(III)Ru(III) core, and therefore, each ruthenium atom donates one electron to the N_2O_2 moiety. Mulliken spin densities are localized at both the ruthenium atoms during the reorientation step in the proton-assisted paths, supporting that all intermediates retain the hyponitrite structure with a N=N double bond. In the HOMO of **A** (**1**) shown in Figure 3a, the π^* orbitals of the two NO ligands overlap in-phase to provide a weak bonding interaction between the nitrogen atoms. On the other hand, the LUMO has a π-bonding character between the nitrogen atoms as well as an antibonding character between the diruthenium core and the N_2O_2 moiety. The two-electron donation induced by the protonation corresponds to the occupation of the LUMO of **1**. As a result, the N—N bond is shortened, and the Ru—N bonds are elongated in **1**[**H**] and **1**[**2H**]. The averaged Ru—N distance is 2.058 Å in **1**[**H**] and 2.100 Å in **1**[**2H**], while the N—N distance is 1.317 Å in **1**[**H**] and 1.270 Å in **1**[**2H**]. These bond distances indicate that **1**[**2H**] has a stronger N=N bond and weaker Ru—N bonds than **1**[**H**]. Since the reorientation step involves the cleavage of a Ru—N bond in **1**, the diprotonated path requires low activation energy compared to the monoprotonated one (17.6 vs 26.2 kcal/mol). These changes in geometric and electronic structures of the N_2O_2 moiety upon protonation allow the proton-assisted models to adopt an energetically more favorable pathway in the reorientation step.

As seen in the LUMO of **1**, the two-electron transfer weakens the bonding between the diruthenium core and the NO ligands. Actually, the protonation of the NO ligands significantly reduces the bond energy between the diruthenium core and the N_2O_2 moiety from 67.4 kcal/mol in **1** to 19.8 kcal/mol in **1**[**2H**]. Although the $Ru(III)_2—(HON{=}NOH)$ bond energy in **1**[**2H**] is higher than the activation energy for the reorientation of the HONNOH ligand bound to the diruthenium core (17.6 kcal/mol), elimination of the HONNOH ligand from the diruthenium core is possible to occur at room temperature. In such a case, the HONNOH molecule might be decomposed into H_2O and N_2O molecules under strongly acidic conditions. The decomposition of HONNOH proceeds in an exergonic way by 35.1 kcal/mol with an activation energy of 15.2 kcal/mol (see Supporting Information Figure S5). Thus, the transition state for the decomposition via the elimination of the HONNOH ligands from the diruthenium core locates 35.0 kcal/mol above **1**[**2H**]. This value is much higher than the highest-energy point ($\mathbf{TS}_{2/5}$[**2H**], 18.2 kcal/mol) in Figure 7.

In the monoprotonated path, the cleavage of the bridging O−N bond of **2**[**H**] leads to the formation of **3**[**H**]. The O−N bond cleavage through the transition state $\mathbf{TS}_{2/3}$[**H**] undergoes a migration of the proton on O^a to form an OH group and N_2O in **3**[**H**]. The activation energy of this step is calculated to be

DOI: 10.1021/acs.inorgchem.5b00394
Inorg. Chem. 2015, 54, 7181−7191

18.2 kcal/mol, which is comparable to that in the proton-free path (17.4 kcal/mol). The release of the N_2O ligand on Ru^b results in the formation of a hydroxido-bridged complex **4**[**H**] via $\mathbf{TS}_{3/4}$[**H**]. The activation energy of 6.4 kcal/mol is lower than that calculated for the proton-free path (12.1 kcal/mol), which may be ascribed to a difference in the formal charge of Ru^b in **3** (+2) and **3**[**H**] (+3). Unlike the case of the proton-free path, spin density distribution is almost unchanged during the O−N bond cleavage and N_2O formation. The total reaction **1**[**H**] → **4**[**H**] + N_2O is exergonic by 29.6 kcal/mol, and thus the monoprotonated path is energetically more favorable than the proton-free path. Arikawa and co-workers reported that the treatment of **4** with HBF_4 in diethyl ether gave the paramagnetic **4**[**H**], and proposed that **4**[**H**] should be involved in the reaction pathway of the NO reduction in the present diruthenium system.[44,45]

In the diprotonated path, the activation energy for the O^b−N^b bond cleavage in **2**[**2H**] is decreased to 11.9 kcal/mol due to the presence of a proton on O^b. The O^b−N^b bond distance (bond order) of 1.410 Å (0.93) indicates that the O^b−N^b bond in **2**[**2H**] is weakened compared with those in **2** (1.344 Å (1.04)) and **2**[**H**] (1.354 Å (1.05)). On the way to the diruthenium aqua−N_2O intermediate **3**[**2H**], we found a metastable intermediate **5**[**2H**] involving Ru−OH and Ru−NNOH moieties. The transition state $\mathbf{TS}_{5/3}$[**2H**] for the hydrogen transfer from the NNOH group to the OH group was successfully located, but the activation barrier is virtually lost after thermal corrections. The release of N_2O from **3**[**2H**] followed by the formation of an aqua-bridged diruthenium complex **4**[**2H**] requires a quite low activation energy of 1.9 kcal/mol, which is lower than the value calculated for the monoprotonated path (6.4 kcal/mol). The total reaction **1**[**2H**] → **4**[**2H**] + N_2O is exergonic by 28.9 kcal/mol. The low activation energy for the release of N_2O in the diprotonated path can be attributed to the destabilization of **3**[**2H**] caused by the steric repulsion between the aqua and N_2O ligands. The O^b−Ru^a−Ru^b−N^b dihedral angle of **3**[**2H**] is 15.5°, while the corresponding dihedral angles of **3**[**H**] and **3** are 6.0° and 0.1°, respectively. In **3**[**H**], the Ru^b−Ru^a−O^b−H dihedral angle is calculated to be 179.4°, and thus the proton on O^b occupies the space remote from the N_2O ligand. We optimized **3′**[**H**], a conformer of **3**[**H**] in which the proton is directed to the N_2O ligand (Ru^b−Ru^a−O^b−H = 52.4°). The O^b−Ru^a−Ru^b−N^b dihedral angle in **3′**[**H**] (16.3°) is very close to that in **3**[**2H**] (15.5°), and **3′**[**H**] is 3.3 kcal/mol less stable than **3**[**H**], which is comparable to the energy difference in the activation barrier for the N_2O elimination between the mono- and diprotonated models (4.5 kcal/mol). The skeletal framework of **3**[**2H**] is distorted by the steric repulsion between the aqua and N_2O ligands on Ru^a and Ru^b, and thereby the N_2O ligand is readily eliminated in the diprotonated model. Arikawa and co-workers did not isolate **4**[**2H**] due to easy deprotonation, but detected its formation by mass spectrometry.[45]

In summary, the protons attached to the NO ligands in **1** effectively assist the reorientation of the N_2O_2 moiety by withdrawing two electrons from the Ru(II)—Ru(II) core. These electrons are stored at the N_2O_2 moiety to fix the hyponitrite structure $(O—N{=}N—O)^{2-}$ with a strong N=N double bond. The fixation of the hyponitrite structure also weakens the Ru—N bonds, and thereby the protonated complexes are allowed to adopt different reaction pathways that require a significant low activation energy for the reorientation step. The following two reaction steps, the cleavage of the O—N bond and the release of N_2O, are expected to proceed smoothly with the aid of protons. The present calculations show that the initial complex **1** should be doubly protonated at least at the first stage of the NO reduction because the reorientation step is still rate-determining in the proton-assisted paths and only the activation energy calculated for the diprotonated system (17.6 kcal/mol) is appropriate for a reaction occurring at room temperature. The free energy change of deprotonation reaction **2**[**2H**] + $CF_3SO_3^-$ → **2**[**H**] + CF_3SO_2OH is calculated to be −23.8 kcal/mol (see Supporting Information Figure S6), suggesting a facile deprotonation of the $N_2O_2H_2$ moiety in the diprotonated O—N-bridged complex. The computational findings are consistent with the experimental fact that a strong acid such as HBF_4 is necessary for the NO reduction on the diruthenium complex. On the other hand, the assistance of protons is not essential except for the reorientation step, and therefore, both the proton-free and proton-assisted mechanisms are also acceptable after the formation of the O—N-bridged intermediates.

4. CONCLUSIONS

We have performed DFT calculations to propose possible reaction pathways of the reduction of NO to N_2O by a dinuclear ruthenium complex, $[(TpRu)_2(\mu\text{-Cl})(\mu\text{-pz})\{\mu\text{-N}(=O)\text{-N}(=O)\text{-}\kappa^2\}]$ (**1** or **A**). On the basis of the experimental fact that the NO reduction proceeds under strongly acidic conditions, the reaction mechanisms were investigated by using three model complexes, where zero to two protons are attached to the NO ligands. The NO ligands in **1** were confirmed to be the most basic sites for both the first and second protonation reactions. The calculated free energy changes for the protonation reactions suggest that one of the NO ligands in **1** would be protonated, and the other can be protonated temporarily in the presence of a strong acid. The mechanism of the NO reduction involves three reaction steps: (i) reorientation of the coordinated NO dimer in **1** to afford an O—N-bridged NO dimer complex, (ii) the O—N bond cleavage to give an intermediate ligating $-O(H)_x$ and −NNO groups, and (iii) the release of N_2O accompanied by the formation of an $O(H)_x$-bridging complex. The calculated results indicate that protons attached to the NO ligands in **1** effectively assist the reorientation of the N_2O_2 moiety by withdrawing two electrons from the Ru(II)—Ru(II) core. These electrons are stored at the N_2O_2 moiety to fix a hyponitrite structure $(O—N{=}N—O)^{2-}$ with a strong N=N double bond. The fixation of the hyponitrite structure simultaneously weakens the Ru−N bonds, and thereby the protonated complexes are allowed to adopt an alternative pathway that requires a significant low activation energy for the reorientation step. The following two reaction steps are also expected to proceed smoothly with the aid of protons. The present calculations suggest that **1** should be doubly protonated at least at the first stage of the NO reduction because the reorientation step is still rate-determining in the proton-assisted paths, and only the activation energy calculated for the diprotonated system (17.6 kcal/mol) is appropriate for the reaction occurring at room temperature. These computational findings are consistent with the experimental fact that a strong acid such as HBF_4 is indispensable for the NO reduction on the diruthenium complex. On the other hand, protons are not necessarily required for the formation of N_2O and resulting $OH_{(x)}$-bridged diruthenium complexes. Our mechanistic study on the diruthenium system demonstrates that protons

DOI: 10.1021/acs.inorgchem.5b00394
Inorg. Chem. 2015, 54, 7181−7191

positively contribute to both the N—N bond formation and N—O bond cleavage toward NO reduction under ambient conditions, and could provide a better insight into the role of protons in the biological NO reduction that proceeds at the diiron active center of s-NOR.

■ ASSOCIATED CONTENT

Supporting Information

Energy diagrams and optimized structures of the reaction species, Mulliken spin densities in the open-shell singlet state, validation of the protonated models, theoretical evaluation of pK_a for the protonated complexes, and Cartesian coordinates of the optimized structures of all the species. The Supporting Information is available free of charge on the ACS Publications website at DOI: 10.1021/acs.inorgchem.5b00394.

■ AUTHOR INFORMATION

Corresponding Authors

*E-mail: arikawa@nagasaki-u.ac.jp.
*E-mail: kazunari@ms.ifoc.kyushu-u.ac.jp.

Notes

The authors declare no competing financial interest.

■ ACKNOWLEDGMENTS

We acknowledge Grants-in-Aid for Scientific Research (Nos. 22245028, 24109014, 24550190, and 26888008) from the Japan Society for the Promotion of Science (JSPS) and the Ministry of Education, Culture, Sports, Science and Technology of Japan (MEXT) and the MEXT Projects of "Integrated Research on Chemical Synthesis" and "Elements Strategy Initiative to Form Core Research Center".

■ REFERENCES

(1) Luchsinger, B. P.; Rich, E. N.; Yan, Y.; Williams, E. M.; Stamler, J. S.; Singel, D. J. *J. Inorg. Biochem.* **2005**, *99*, 912−921.
(2) Feng, C.; Tollin, G.; Hazzard, J. T.; Nahm, N. J.; Guillemette, J. G.; Salerno, J. C.; Ghosh, D. K. *J. Am. Chem. Soc.* **2007**, *129*, 5621−5629.
(3) de Mel, A.; Murad, F.; Seifalian, A. M. *Chem. Rev.* **2011**, *111*, 5742−5767.
(4) Enemark, J. H.; Feltham, R. D. *Coord. Chem. Rev.* **1974**, *13*, 339−406.
(5) Serres, R. G.; Grapperhaus, C. A.; Bothe, E.; Bill, E.; Weyhermüller, T.; Neese, F.; Wieghardt, K. *J. Am. Chem. Soc.* **2004**, *126*, 5138−5153.
(6) Kaim, W.; Schwederski, B. *Coord. Chem. Rev.* **2010**, *254*, 1580−1588.
(7) Wright, A. M.; Hayton, T. W. *Comments Inorg. Chem.* **2012**, *33*, 207−248.
(8) Singh, P.; Das, A. K.; Sarkar, B.; Niemeyer, M.; Roncaroli, F.; Olabe, J. A.; Fiedler, J.; Záliš, S.; Kaim, W. *Inorg. Chem.* **2008**, *47*, 7106−7113.
(9) Yamaguchi, M.; Arikawa, Y.; Nishimura, Y.; Umakoshi, K.; Onishi, M. *Chem. Commun.* **2009**, 2911−2913.
(10) Lehnert, N.; Scheidt, W. R.; Wolf, M. W. *Struct. Bonding (Berlin)* **2014**, *154*, 155−224.
(11) Evans, W. J.; Fang, M.; Bates, J. E.; Furche, F.; Ziller, J. W.; Kiesz, M. D.; Zink, J. I. *Nat. Chem.* **2010**, *2*, 644−647.
(12) Hino, T.; Matsumoto, Y.; Nagano, S.; Sugimoto, H.; Fukumori, Y.; Murata, T.; Iwata, S.; Shiro, Y. *Science* **2010**, *330*, 1666−1670.
(13) Moënne-Loccoz, P. *Nat. Prod. Rep.* **2007**, *24*, 610−620.
(14) Wasser, I. M.; de Vries, S.; Moënne-Loccoz, P.; Schröder, I.; Karlin, K. D. *Chem. Rev.* **2002**, *102*, 1201−1234.
(15) Suharti; Strampraad, M. J. F.; Schröder, I.; de Vries, S. *Biochemistry* **2001**, *40*, 2632−2639.
(16) Pinakoulaki, E.; Varotsis, C. *J. Inorg. Biochem.* **2008**, *102*, 1277−1287.
(17) Pinakoulaki, E.; Stavrakis, S.; Urbani, A.; Varotsis, C. *J. Am. Chem. Soc.* **2002**, *124*, 9378−9379.
(18) Butler, C. S.; Seward, H. E.; Greenwood, C.; Thomson, A. J. *Biochemistry* **1997**, *36*, 16259−16266.
(19) Schopfer, M. P.; Wang, J.; Karlin, K. D. *Inorg. Chem.* **2010**, *49*, 6267−6282.
(20) Collman, J. P.; Yan, Y.-L.; Lei, J.; Dinolfo, P. H. *Inorg. Chem.* **2006**, *45*, 7581−7583.
(21) Collman, J. P.; Yang, Y.; Dey, A.; Decréau, R. A.; Ghosh, S.; Ohta, T.; Solomon, E. I. *Proc. Natl. Acad. Sci. U. S. A.* **2008**, *105*, 15660−15665.
(22) Dey, S. G.; Dey, A. *Dalton. Trans.* **2011**, *40*, 12633−12647.
(23) Harris, D. L. *Int. J. Quantum Chem.* **2002**, *88*, 183−200.
(24) Coppens, P.; Novozhilova, I.; Kovalevsky, A. *Chem. Rev.* **2002**, *102*, 861−883.
(25) Blomberg, L. M.; Blomberg, M. R. A.; Siegbahn, P. E. M. *Biochim. Biophys. Acta, Bioenerg.* **2006**, *1757*, 240−252.
(26) Blomberg, M. R. A.; Siegbahn, P. E. M. *Biochemistry* **2012**, *51*, 5173−5186.
(27) Arikawa, Y.; Onishi, M. *Coord. Chem. Rev.* **2012**, *256*, 468−478.
(28) Shoji, M.; Hanaoka, K.; Kondo, D.; Sato, A.; Umeda, H.; Kamiya, K.; Shiraishi, K. *Mol. Phys.* **2014**, *112*, 393−397.
(29) Pinakoulaki, E.; Ohta, T.; Soulimane, T.; Kitagawa, T.; Varotsis, C. *J. Am. Chem. Soc.* **2005**, *127*, 15161−15167.
(30) Girsch, P.; de Vries, S. *Biochim. Biophys. Acta, Bioenerg.* **1997**, *1318*, 202−216.
(31) Matsumura, H.; Hayashi, T.; Chakraborty, S.; Lu, Y.; Moënne-Loccoz, P. *J. Am. Chem. Soc.* **2014**, *136*, 2420−2431.
(32) Silaghi-Dumitrescu, R.; Kurtz, D. M., Jr.; Ljungdahl, L. G.; Lanzilotta, W. N. *Biochemistry* **2005**, *44*, 6492−6501.
(33) Kurtz, D. M., Jr. *Dalton. Trans.* **2007**, 4115−4121.
(34) Blomberg, L. M.; Blomberg, M. R. A.; Siegbahn, P. E. M. *JBIC, J. Biol. Inorg. Chem.* **2007**, *12*, 79−89.
(35) Caranto, J. D.; Weitz, A.; Hendrich, M. P.; Kurtz, D. M., Jr. *J. Am. Chem. Soc.* **2014**, *136*, 7981−7992.
(36) Zheng, S.; Berto, T. C.; Dahl, E. W.; Hoffman, M. B.; Speelman, A. L.; Lehnert, N. *J. Am. Chem. Soc.* **2013**, *135*, 4902−4905.
(37) Shiotari, A.; Hatta, S.; Okuyama, H.; Aruga, T. *Chem. Sci.* **2014**, *5*, 922−926.
(38) Flock, U.; Lachmann, P.; Reimann, J.; Watmough, N. J.; Ädelroth, P. *J. Inorg. Biochem.* **2009**, *103*, 845−850.
(39) Shapleigh, J. P.; Payne, W. J. *J. Bacteriol.* **1985**, *163*, 837−840.
(40) Salomonsson, L.; Reimann, J.; Tosha, T.; Krause, N.; Gonska, N.; Shiro, Y.; Ädelroth, P. *Biochim. Biophys. Acta, Bioenerg.* **2012**, *1817*, 1914−1920.
(41) Varotsis, C.; Ohta, T.; Kitagawa, T.; Soulimane, T.; Pinakoulaki, E. *Angew. Chem., Int. Ed.* **2007**, *46*, 2210−2214.
(42) Ohta, T.; Kitagawa, T.; Varotsis, C. *Inorg. Chem.* **2006**, *45*, 3187−3190.
(43) Sajith, P. K.; Shiota, Y.; Yoshizawa, K. *ACS Catal.* **2014**, *4*, 2075−2085.
(44) Arikawa, Y.; Asayama, T.; Moriguchi, Y.; Agari, S.; Onishi, M. *J. Am. Chem. Soc.* **2007**, *129*, 14160−14161.
(45) Arikawa, Y.; Matsumoto, N.; Asayama, T.; Umakoshi, K.; Onishi, M. *Dalton Trans.* **2011**, *40*, 2148−2150.
(46) Frisch, M. J.; Trucks, G. W.; Schlegel, H. B.; Scuseria, G. E.; Robb, M. A.; Cheeseman, J. R.; Scalmani, G.; Barone, V.; Mennucci, B.; Petersson, G. A.; Nakatsuji, H.; Caricato, M.; Li, X.; Hratchian, H. P.; Izmaylov, A. F.; Bloino, J.; Zheng, G.; Sonnenberg, J. L.; Hada, M.; Ehara, M.; Toyota, K.; Fukuda, R.; Hasegawa, J.; Ishida, M.; Nakajima, T.; Honda, Y.; Kitao, O.; Nakai, H.; Vreven, T.; Montgomery, J. A., Jr.; Peralta, J. E.; Ogliaro, F.; Bearpark, M.; Heyd, J. J.; Brothers, E.; Kudin, K. N.; Staroverov, V. N.; Keith, T.; Kobayashi, R.; Normand, J.; Raghavachari, K.; Rendell, A.; Burant, J. C.; Iyengar, S. S.; Tomasi, J.; Cossi, M.; Rega, N.; Millam, N. J.; Klene, M.; Knox, J. E.; Cross, J. B.; Bakken, V.; Adamo, C.; Jaramillo, J.; Gomperts, R.; Stratmann, R. E.; Yazyev, O.; Austin, A. J.; Cammi, R.; Pomelli, C.; Ochterski, J. W.;

DOI: 10.1021/acs.inorgchem.5b00394
Inorg. Chem. 2015, 54, 7181−7191

Martin, R. L.; Morokuma, K.; Zakrzewski, V. G.; Voth, G. A.; Salvador, P.; Dannenberg, J. J.; Dapprich, S.; Daniels, A. D.; Farkas, O.; Foresman, J. B.; Ortiz, J. V.; Cioslowski, J.; Fox, D. J. *Gaussian 09, Revision C.01*; Gaussian, Inc.: Wallingford, CT, 2010.
(47) Becke, A. D. *Phys. Rev. A: At., Mol., Opt. Phys.* **1988**, *38*, 3098−3100.
(48) Becke, A. D. *J. Chem. Phys.* **1993**, *98*, 5648−5652.
(49) Lee, C.; Yang, W.; Parr, R. G. *Phys. Rev. B: Condens. Matter Mater. Phys.* **1988**, *37*, 785−789.
(50) Andrae, D.; Häußermann, U.; Dolg, M.; Stoll, H.; Preuß, H. *Theor. Chim. Acta* **1990**, *77*, 123−141.
(51) Dunning, T. H.; Hay, P. J. In *Modern Thoretical Chemistry*; Schaefer, H. F., III, Ed.; Plenum: New York, 1976; Vol. 3, pp 1−27.
(52) Fukui, K. *J. Phys. Chem.* **1970**, *74*, 4161−4163.
(53) Fukui, K. *Acc. Chem. Res.* **1981**, *14*, 363−368.
(54) Gonzalez, C.; Schlegel, H. B. *J. Phys. Chem.* **1990**, *94*, 5523−5527.
(55) Miertuš, S.; Scrocco, E.; Tomasi, J. *Chem. Phys.* **1981**, *55*, 117−129.
(56) *Handbook of Chemistry and Physics*, 72nd ed.; Lide, D. R., Ed.; CRC Press: Boca Raton, FL, 1991−1992.
(57) Mayer, I. *Chem. Phys. Lett.* **1983**, *97*, 270−274.
(58) Mayer, I. *Int. J. Quantum Chem.* **1984**, *26*, 151−154.
(59) Merkle, A. C.; McQuarters, A. B.; Lehnert, N. *Dalton Trans.* **2012**, *41*, 8047−8059.
(60) Kütt, A.; Rodima, T.; Saame, J.; Raamat, E.; Mäemets, V.; Kaljurand, I.; Koppel, I. A.; Garlyauskayte, R. Y.; Yagupolskii, Y. L.; Yagupolskii, L. M.; Bernhardt, E.; Willner, H.; Leito, I. *J. Org. Chem.* **2011**, *76*, 391−395.
(61) As a preliminary result, we have confirmed that treatment of **1** with 2.1 equiv of HBF_4 afforded **4** in 19% yield. In addition, treatment of **1** with 2.1 equiv of CF_3SO_2OH afforded **4** in 29% yield.
(62) We also tested other functionals, such as B3LYP*[63] and M06, but all of them gave the same results as the B3LYP functional, where the open-shell singlet state is energetically more favorable.
(63) Reiher, M.; Salomon, O.; Hess, B. A. *Theor. Chem. Acc.* **2001**, *107*, 48−55.

DOI: 10.1021/acs.inorgchem.5b00394
Inorg. Chem. 2015, 54, 7181−7191